Cellulose based fluorescent macromolecular sensors and their ability in 2, 4, 6-trinitrophenol detection

Xinyue Jiao
Wuhan Institute of Technology
Heyi Li
Wuhan Institute of Technology
Xinjian Cheng (chxj606@163.com)
Wuhan Institute of Technology https://orcid.org/0000-0001-9884-4794

Research Article

Keywords: Cellulose derivatives, fluorescence, sensor, trinitrophenol (TNP)

Posted Date: March 11th, 2021

DOI: https://doi.org/10.21203/rs.3.rs-269901/v1

Version of Record: A version of this preprint was published at Materials Today Chemistry on December 1st, 2021. See the published version at https://doi.org/10.1016/j.mtchem.2021.100615.

Abstract

This article deals with three cellulose-based fluorescent macromolecular sensors by introducing 1,8-naphthimide fluorophore to cellulose. Firstly, through the etherification reaction of cellulose with $BrCH_2CH_2NH_2$, $-NH_2$ group bearing cellulose **CS 1** was obtained. And then $-NH_2$ group reacts with 4-bromo-1,8-naphthalic anhydride to synthesize a naphthalimide cellulose derivative (**CS 2**). Finally, recognition group was introduced by substituting Br atoms, and three cellulose fluorescent probes (**CS 3**, **CS 4**, **CS 5**) were obtained eventually. Structure and fluorescence properties of the macromolecular sensors were characterized and confirmed. Fluorescence detection measurements show that these probes can be used as selective and sensitive fluorescent sensors to 2,4,6-trinitrophenol (TNP). The detection limits are 0.52μM, 0.76μM and 0.81μM, respectively, indicating good detection performance. This work provides a new method for the selective detection of TNP and also a method to enlarge the application scope of cellulose.

Highlights

Novel cellulose-based fluorescent sensors were prepared.

The as-prepared macromolecular sensors have selectivity and sensitivity to TNP.

1. Introduction

As an important reagent in chemical industry such as dyes and pesticides, nitroaromatic compounds are widely used (Dhiman et al. 2020). Due to its toxicity and non-degradability, the excessive use will cause irreversible harms to the soil and water(Cheng et al. 2019). It leads to irritation, skin allergies, anemia, carcinogenicity, liver and kidney damage and a series of health problems to human beings as well (Guo et al. 2020; Wang et al. 2020b; Xu et al. 2020). At the same time, these chemicals are also the main component of explosives and often endanger social security. Therefore, it is necessary to develop and improve rapid real-time monitoring and on-site detection methods for such chemicals (Saini et al. 2020). This requires the detector to have the virtue of high sensitivity, good reliability, low detection limit, convenient carrying and easy operation (Xiao et al. 2020; Xiong et al. 2019).

At present, the common methods for nitroaromatic compounds detection are divided into instrumental analysis and chemical reagent detection (Bora et al. 2019). Compared with traditional instrument detection methods such as mass spectrometry (MS), high performance liquid chromatography (HPLC) and electrochemical analysis, the detection sensitivity of chemical reagents is higher, and the pretreatment methods are simple (Guo et al. 2017; Gupta et al. 2017). It is expected to be used for real-time and rapid monitoring of nitroaromatic compounds and attracts attention. Among them, fluorescence detection technology has the advantages of high sensitivity, strong specificity, fast response, and portability, which has attracted much attention (Peretz et al. 2019; Tripathi et al. 2017; Yang et al. 2019). Fluorescent polymers have been synthesized and used in the detection of trace nitroaromatic chemicals.

For example, a triazole-methane-anthracene-functionalized fluorescence quenching polyaromatic chemical sensor was synthesized, which can detect 2,4,6-trinitrophenol (TNP) efficiently and quickly (Qiu et al. 2020). Water-dispersible fluorescent molybdenum disulfide (MoS_2) quantum dots (QDs) capped with 1,4-diaminobutane (DAB) can be used for the selective detection of explosive TNP up to a limit of detection of 5 μM (Sharma and Mehata 2020). A coordination polymer $[Pb(L)_2]_n$ was successfully generated, which can be used as a luminescence sensor for TNP with low detection limit as well (Miao 2019).

Cellulose is considered to be the main raw material of the world's energy and chemical industry due to its abundant sources, non-toxic, non-polluting, easy to modify, and good biocompatibility (Fan et al. 2020; Huang et al. 2020). As a polyhydroxyl linear polymer, cellulose could undergo typical etherification (You et al. 2013), esterification (Kusuma et al. 2019), oxidation (Imamura et al. 2020) and other reactions (Fuchs and Zhang 2019). These reactions endow functional cellulose derivatives being easily prepared, and expanding the application of cellulose (Jasmani et al. 2016). Amino group was introduced by 3-amino-propyltriethoxysilane (APTES) and then grafted to the lignin surface by amidation reaction between the amino group and 1-pyrrolidine butyric acid (PBA), showing obvious fluorescence signal (Xiong et al. 2016). By amidation reaction, Rhodamine B modified with *N*-hydroxysuccinimide was labeled on cellulose nanofibers (Navarro and Bergstrom 2014). Via combination of fluorescent 1,8-naphthalimide and cellulose nanocrystalline (CNCs), the application in Pb^{2+} sensing was further explored (Song et al. 2019). However, due to the large number of hydrogen bonds and intermolecular interactions in the cellulose chain, it is still a challenge to prepare fluorescent cellulose derivatives with good solubility (Barazzouk and Daneault 2011).

1,8-Naphthimide has the following characteristics: coplanarity; a larger conjugated system; one section of the molecule has a strong electron-donating group, and the other end has a strong electron-withdrawing group (Choi et al. 2016; Li et al. 2020). The electrons in this system are easily irradiated by light to undergo transitions, thereby generating fluorescence. Furthermore, the introduction of different groups on the naphthalene ring can greatly change the fluorescent properties of such fluorophores. They are widely used in chemical sensors, molecular switches, fluorescent probes, lasers and other fields (Bahta and Ahmed 2019).

In this work, $BrCH_2CH_2NH_2$ was successfully introduced into the cellulose backbone (**CS 1**) by Williamson synthesis firstly. And then it reacted with 4-bromo-1, 8-naphthalenedicarboxylic acid anhydride to synthesize naphthalimide fluorescent cellulose derivative (**CS 2**). Finally, three cellulose-based fluorescence sensors (**CS 3**, **CS 4**, **CS 5**) were synthesized by introducing different electron-rich moieties as 2-mercaptobenzothiazole, benzothiazole-2-ylamine and 2-mercaptobenzimidazole. The results show that the new fluorescent cellulose derivatives have potential applications in the field of chemical sensing.

2. Experimental

4-bromo-1,8-naphthalic anhydride, Cellulose pulp powder (50 μm), Butylamine, 2-Bromoethylamine Hydrobromide, Benzyltriphenylphosphonium hydroxide, 2-Mercaptobenzothiazole, Benzothiazole-2-ylamine, 2-Mercaptobenzimidazole were purchased from J&K China Chemical Ltd.

Nitrobenzene (NB), 4-nitrochlorobenzene (4-NCB), benzoic acid (BA), 3,5-dinitrobenzoic acid (DNBA), aniline (AN), methylbenzene (MB), 4-nitrotoluene (4-NT), phenol (NP), 4-nitrophenol (4-NP), 2,4,6-trinitrophenol (TNP), potassium hydroxide and potassium carbonate are purchased from Aladdin Chemical Co. Ltd. dimethyl sulfoxide (DMSO), *N*,*N*-dimethylformamide (DMF), ethanol, acetonitrile, acetone were purified by distillation for further use.

2.2. Instrumentation

Fourier transform infrared spectroscopy (FTIR, 4000–400 cm^{-1}, Thermo Fisher, USA) was measured by Nicolet 6700 instrument. The sample was prepared by the standard KBr particle method. ^1H NMR was measured on AVANCE III 600 MHz (Bruker, Switzerland) instrument (in $CDCl_3$, d_6-DMSO). The elemental, content and binding energy were measured by X-ray photoelectron spectroscopy (XPS, PHI-5300; ESCA PHI China Limited company, Beijing). The microscopic morphologies were obtained by scanning electron microscopy (SEM, JSM-5510LV, Japan). Thermogravimetric analysis (TGA) and differential scanning calorimeter (DSC) were acquired by STA449F3 instrument (NETZSCH, German). UV absorption spectra were measured on a UV-5900PC spectrophotometer (METASH, shanghai, China). Fluorescence spectra were performed on a Shimadzu F-4500 (Shimadzu, Shanghai Global Laboratory Consumables Co., Ltd.) fluorescence spectrophotometer.

2.3. Synthesis

Cellulose derivatives (**CS 1**, **CS 2**, **CS 3**, **CS 4** and **CS 5**, their structures could be seen in Scheme 1) containing functional monomer naphthalimide groups were prepared, and the synthesis routes were shown in scheme 1. In order to further prove that the partial structure of the above-mentioned fluorophores can be synthesized readily, as reference molecules, *n*-butylamine instead of compound **CS 1** was used to synthesize small fluorescent probe molecules (**AC 2**, **AC 3**, **AC 4** and **AC 5**, their structures could be seen in Scheme 2).

2.3.1. Synthesis of CS 1

CS 1 was synthesized according to the literature (Abe et al. 2017). Firstly, cellulose powder (0.1 g) was dissolved in $[P_{4,4,4,4}]OH$ aq. solution and stirred at 25°C in an atmosphere of nitrogen for 30 minutes. Then 2-Bromoethylamine Hydrobromide (0.55 g) were added to the cellulose solution and reacted at 60°C for 24 h under nitrogen atmosphere. Afterwards, the reaction product was precipitated, washed with water and ethanol, and then vacuum dried at 35°C for 24 hours to obtain the product (0.08 g; 80% yield).

^1H NMR (600 MHz, DMSO, ppm): δ 5.74 (s, bromoethylamine H-9), 3.02 (s, cellulose H-1, 2, 3), 2.65 (s, cellulose H-4, 5), 2.53 (s, cellulose H-6).

2.3.2. Synthesis of CS 2

CS 1 (0.1 g) was suspended in 10 mL dry DMF at 25℃, followed by several drops of 4-bromo-1,8-naphthalic anhydride (0.2 g). The mixture was recycled at nitrogen gas at 80℃ for 14 hours, cooled to room temperature (Hu et al. 2018). The solids were precipitated and washed with DMF and acetone to get 0.09 g brownish powder **CS 2** (yield 90%).

^{1}H NMR (600 MHz, DMSO, ppm): δ 8.29 (s, naphthalimide H-9,10,11,12,13), 4.56 (s, ethylamine H-7, 14), 4.22 (s, ethylamine H-8), 3.00 (s, cellulose H-1, 2, 3, 4, 5), 2.53 (s, cellulose H-6).

2.3.3. Synthesis of CS 3, CS 4 and CS 5.

CS 2 (0.1 g), 2-Mercaptobenzothiazole (0.7 g) and potassium carbonate (0.4 g) were suspended in dry DMF and stirred at 85℃ for 14 h (Ruiz-Sanchez et al. 2020). Yellow precipitated material was filtered and the residual 2-mercaptobenzothiazole on the solid was washed away by using an excess of acetone. The final residue was dried in vacuum to obtain 0.085 g yellow solid of **CS 3**. Similarly, we successfully synthesized polymers **CS 4** and **CS 5** using the same method. **CS 4** is a brown solid with a yield of 87%, and **CS 5** is a yellow solid with a yield of 90%.

CS 3: ^{1}H NMR (600 MHz, DMSO, ppm): δ 8.10 (s, naphthalimide H-9,10,11,12,13), 7.93 (s, mercaptobenzothiazole H-14,15,16,17), 4.67 (s, ethylamine H-8, 18) 3.85(s, ethylamine H-7), 3.02 (s, cellulose H-1, 2, 3), 2.65 (s, cellulose H-4, 5), 2.53 (s, cellulose H-6).

CS 4: ^{1}H NMR (600 MHz, DMSO, ppm): δ 8.29 (s, naphthalimide H-9,10,11,12,13), 7.93 (s, aminobenzothiazole H-14,15,16,17), 4.65 (s, ethylamine H-8, 18) 3.76 (s, ethylamine H-7), 2.86 (s, cellulose H-1, 2, 3), 2.69 (s, cellulose H-4, 5), 2.62 (s, cellulose H-6).

CS 5: ^{1}H NMR (600 MHz, DMSO, ppm): δ 8.37 (s, naphthalimide H-9,10,11,12,13), 7.93 (s, mercaptobenzimidazole H-14,15,16,17), 4.25 (s, ethylamine H-8, 18), 3.87 (s, ethylamine H-7), 2.87 (s, cellulose H-1, 2), 2.71 (s, cellulose H-3), 2.65 (s, cellulose H-4, 5), 2.53 (s, cellulose H-6).

3. Results And Discussion

3.1. Design and synthesis

1,8-Naphthimide fluorescent dyes are a very important class of fluorescent reagent, which exhibit good colorimetric and fluorescent reactions in biological assays and other specific photophysical studies, and have high light stability and quantum yield. There are a large number of hydrogen bonds in cellulose molecules, which are easy to form complex intermolecular and intramolecular bonds, with high crystallinity. Once naphthalimide was attached to the cellulose chain for modification and functionalization, cellulose-based fluorescent macromolecular sensor could be synthesized. Scheme 1 shows the synthesis steps of cellulose fluorescent probe. The cellulose-based fluorescent polymer

derivatives were characterized by FTIR and XPS, and further characterized by SEM, TGA, DSC and fluorescence spectroscopy. Similarly, small fluorescent probe molecules (**AC 2**, **AC 3**, **AC 4** and **AC 5**) were characterized by FTIR, ^{1}H NMR, MS, seeing the supporting information. (Fig. S1-S5).

3.2. Structure of fluorescent celluloses

3.2.1. FTIR analysis

The FTIR spectra of cellulose and their derivatives are shown in Fig. 1(a). It can be seen that original **CS** has a strong peak at about 3439 cm^{-1}, which is related to the large amount of -OH on the cellulose chain. The tensile vibration of C-H is around 2910 cm^{-1}. For **CS 1**, the peak at 1254 cm^{-1} is attributed to the vibration of the C-N bond, and the wider peak at 894 cm^{-1} to 707 cm^{-1} belongs to the out-of-plane bending vibration of the amino group, which indicates that the amino group has been successfully grafted onto cellulose. When naphthalimide moiety was introduced, a new peak of **CS 2** appeared at 521 cm^{-1}, which was caused by C-Br stretching; at the same time, the absorption peaks at 1374 cm^{-1} and 790 cm^{-1} indicated the presence of a naphthalene ring. The peak at 1630 cm^{-1}represented the stretching vibration of carbonyl groups (-C = O). Since the benzothiazole nucleophiles substituted for Br on the naphthalimide are similar, the peaks appearing in the FTIR spectra are not particularly obvious. For **CS 3**, **CS 4**, and **CS 5**, the absorption peak around 1066 cm^{-1}, which is an absorption peak of the C-S-C stretching vibration. These phenomena confirm that the compounds **CS 3**, **CS 4**, **CS 5** have been synthesized.

3.2.2. ^{1}H NMR analysis

Cellulose is difficult to dissolve in DMSO, but through a series of modification reactions, its condensed state is destroyed, making it more soluble in the polar solvent DMSO. Therefore, ^{1}H NMR spectrum have been made to analysis its structure. Figure 1 displays the ^{1}H NMR spectra of cellulose derivatives in DMSO-d_6. As can be seen, typical peaks at 2.53–3.02 ppm could be assigned as the unit of cellulose (H1, H2, H3, H4, H5, H6), peaks at 4.22 ppm are responsible for amino (H18). after reacted with naphthalimide, peaks at 8.37 ppm could be assigned to naphthalimide. After substitution reaction, peaks at 7.93 ppm could be assigned to benzothiazole groups (H14, H15, H16, H17).

3.2.3. XPS analysis

X-ray photoelectron spectroscopy (XPS) was used to further measure the chemical composition of cellulose derivatives. As we all know, **CS** is composed of three elements: H, C, and O, combining with the naphthalimide, other elements will be introduced. The element content of each component is shown in Table 1. Peak signal for each element could be seen in SI (Table S1). Combining Table 1 and Table S1, the cellulose spectra have two peaks near 285 eV and 532 eV, corresponding to C1 and O1, respectively. For **CS 1**, a new peak appears at 70 eV, indicating that the amino group has been successfully introduced. When naphthalimide was introduced, **CS 2** exhibits a new bromine peak (Br 3d). When 2-mercaptobenzothiazole was connected, the Br peak (Br 3d) disappeared, a new sulfur peak (S 2p)

appeared, and the O and C content in the molecule has also changed. For the other two samples **CS 4** and **CS 5**, new sulfur peaks (Br 3d) also appeared, which can prove the successful substitution reaction on the cellulose surface. The degree of substitution (DS) refers to the amounts of substances in which the active hydroxyl groups on each glucose unit of cellulose are substituted. Since 3 hydroxyl groups on each dehydrated glucose unit in the cellulose molecular chain can be substituted at most, the degree of substitution is between 0 to 3. According to the data in Table 1, it is roughly determined that there is one naphthalimide group in 14 glucose units, and one recognition group in 25 glucose units (such as benzothiazole groups). Therefore, by definition, the DS value of the cellulose substituent is calculated by the following equation:

$$DS = \frac{n_{substitution\ group}}{n_{glucose\ unit}} \quad (1)$$

The DS of naphthalimide groups ($DS_{CS\,2}$) was calculated to be 0.07 and the DS of benzothiazole groups ($DS_{CS\,3}$) was calculated to be 0.04.

Table 1
The content of elemental components in cellulose samples by XPS.

Atomic %	CS	CS 1	CS 2	CS 3	CS 4	CS 5
C	57.65	60.66	70.27	61.68	57.78	59.37
O	42.35	38.25	26.65	37.2	41.29	39.5
N	-	1.09	2.59	0.8	0.73	1.02
Br	-	-	0.49	-	-	-
S	-	-	-	0.33	0.19	0.11

3.2.4. SEM analysis

Scanning electron microscope (SEM) was used to analyze the microstructure of cellulose and determine the structural changes of cellulose. It can be clearly seen that the original **CS** is long rod-shaped and its surface is smooth (Fig. 2(a)). Because **CS** dissolves in $[P_{4,4,4,4}]OH$ aq. solution, it will cause surface changes. It can be seen from Fig. 2(b) that after the reaction, the surface becomes rough and loose (Luo et al. 2019). The SEM of **CS 2** and **CS 3** are shown in Fig. 2(c) and Fig. 2(d). Because cellulose undergoes a series of reactions, fluorescent groups are introduced, which destroyed the regular structure of the cellulose chain and reduces the crystallinity degree of cellulose. Therefore, cellulose derivatives are not as easy to crystallize as before, and the aggregate structure becomes loose. It can be seen that the cellulose gradually became rough from the original smooth surface, leaving many pores on the surface, which increases the specific surface area of the cellulose and makes it easier to combine with analytes. The

SEM of **CS 4** and **CS 5** are shown in the supporting information. (Fig. S6). Many physical and chemical properties of the modified cellulose molecules have been improved by this way (Wang et al. 2020a).

3.2.5. TGA and DSC analysis

The TGA curves are shown in Fig. 3(a), and the thermal analysis data is summarized as well. As shown in the figure, the weight of the four samples decreased at around 100°C, which was caused by the loss of adsorbed water and volatile substances. Because there are many intramolecular hydrogen bonds on cellulose macromolecules, cellulose has high heat resistance (de Faria et al. 2017), and the sample **CS** loses weight rapidly at 320°C. When fluorescent monomers are attached to cellulose, the decomposition temperature of cellulose decreases, sample **CS 3**, **CS 4**, and **CS 5** begin to lose weight at 280°C. This may be due to the fact that the inserted substituents have destroyed part of the original rigid structure. It's about 350°C, most of the sample has been decomposed. When the temperature exceeds 400°C, the biomass of the cellulose derivative decreases uniformly, and at the same time, it can be seen from the table in Fig. 3(a) that the cellulose-modified derivative shows a higher residual mass than the cellulose raw material. This also shows that the organic compound is successfully grafted onto the cellulose chain.

The DSC curve was used to evaluate the modified cellulose macromolecules, and shown in Fig. 3(b). The DSC of the original material cellulose **CS** showed that the glass transition temperature (T_g) was about 339°C. After modification, the T_g of cellulose derivative samples **CS 3**, **CS 4**, and **CS 5** were 340℃, 337℃ and 327℃, respectively. Due to the influence of the substituents, part of the hydrogen bonds and intermolecular interactions are destroyed, which reduces the degree of cross-linking of the cellulose molecular chain, but the proportion of fluorescent molecules introduced is not large, so the Tg is slightly reduced. In this study, the measured DSC data is close to the TGA data, indicating that the two systems have good consistency.

3.3. Detection of aromatic and aromatic nitro compounds

Using the sensing properties of cellulose naphthalimide derivative macromolecular fluorescent probes, 10 kinds of aromatic and aromatic nitro compounds, nitrobenzene (NB), 4-nitrochlorobenzene (4-NCB), benzoic acid (BA), 3,5-dinitrobenzoic acid (DNBA), aniline (AN), methylbenzene (MB), 4-nitrotoluene (4-NT), phenol (NP), 4-nitrophenol (4-NP), 2,4,6-trinitrophenol (TNP) were tested. Cellulose is difficult to dissolve in common solvents such as acetonitrile and ethanol. Therefore, we choose DMSO with greater polarity as the solvent, grind the product into a fine powder, and dissolve the product after ultrasonic mixing. 10 aromatic and aromatic nitro compounds were added to the cellulose fluorescent probe solution, and the UV-vis spectra and fluorescence spectra of the mixed solution were recorded. After testing, in addition to polymer **CS 4** has the ability to recognize 4-NP and TNP, **CS 3**, **CS 5** have specific recognition ability to TNP.

Figure 4(a) shows the fluorescence emission spectra of **CS 3** in the presence of nitro-aromatic compounds (50μM). It can be seen from Fig. 4(a) that the fluorescence intensity is significantly reduced

after adding TNP, which is about two-thirds reduction, while the fluorescence intensity is basically unchanged when other aromatic compounds are added. Therefore, the selectivity of quenching by TNP is higher than that of other aromatic compounds. This indicates that the fluorescent probe **CS 3** has good selectivity for TNP. The UV-Vis spectra of Fig. S8(a) includes naphthalimide units, which are characterized by a distinct absorption band at 365 nm. Since the low-concentration TNP solution is yellow-green, when TNP is added, the absorbance increases, the absorption peak also changes, and the color of the solution changes from colorless to yellow-green. When 4-NP was added to the **CS 3** solution, the maximum absorption wavelength blue shifted from 365 nm to 320 nm, and the absorbance also increased slightly. But when other nitro compounds were added, the UV-Vis spectra of **CS 3** remained basically unchanged, and the color of the solution didn't change significantly.

Figure 4(b) shows the change of the fluorescence intensity of compound **CS 3** *vs* the concentration of TNP. After adding TNP to the polymer solution, the fluorescence of the solution decreased significantly. As the concentration of TNP increased, the fluorescence intensity first showed a linear downward trend and then became slower. The photo of the sensor **CS 3** performing the fluorescence titration on all the test objects is shown in Fig. S11, and the change trend is consistent with the actual measured data. Therefore, the fluorescence quenching of **CS 3** in DMSO solution can quantitatively detect TNP. The standard slope is obtained from the linear relationship diagram of **CS 3** in Fig. 4(c), and the detection limit of the sensor is obtained according to the limit detection (LOD) calculation formula. As a result, the detection limit was calculated to be 0.52 μM.

It can be seen from Fig. 5(a) that the maximum emission peak of **CS 4** is 453nm, and fluorescnece quenched by 4-NP and TNP after adding 10 different aromatic nitro compounds. Among them, 4-NP quenched half of it, and the addition of TNP quenched up to 75%. Similar to **CS 3**, when **CS 4** encounters nitroaromatic compounds, the UV-vis spectra of TNP shifts from 343 nm to 356 nm, and the UV absorption is significantly enhanced. The spectral absorption peak of 4-NP moves to 310nm, and the ultraviolet absorption is also slightly enhanced. (Fig. S8).

In order to determine the detection limit of the cellulose-based probes for TNP and 4-NP, Fig. 5(c) and Fig. 5(d) record the fluorescence spectra under different concentrations of 4-NP and TNP. As could be seen, the fluorescence intensity of **CS 4** decreases with the increase of the concentration of nitro compounds. The lowest concentrations of TNP and 4-NP that can be recognized by **CS 4** are 5μM and 10μM, respectively. When **CS 4** meets nitro compounds at this concentration, the fluorescence change can still be seen (Fig. S11). When 60μM TNP was added, the fluorescence intensity of the sensor solution was quenched by about 80%; when 110μM 4-NP was added, the fluorescence reached the complete quenched state. It can be seen from the three aspects of fluorescence spectra, UV-vis spectrum and color change that this probe is a better choice for detecting 4-NP and TNP. As shown in Fig. 5(d) and 5(e), the standard curve of TNP and 4-NP are obtained. The limit of detection (LOD) of probe **CS 4** for TNP and 4-NP were calculated as 0.76μM and 1.5μM, respectively. This result indicates that **CS 4** is more sensitive to TNP.

By adding a series of nitro-aromatic compounds, the fluorescence emission spectra and UV-vis spectra are obtained and shown in Fig. 6(a) and Fig. S8(c). Compound **CS 5** emits fluorescence with a maximum wavelength of 455 nm under excitation of 365 nm. It can be seen that upon adding of TNP, the fluorescence intensity of **CS 5** is about 70% quenched. Except TNP, the presence of other aromatic nitro compounds didn't cause notable changes. It shows that **CS 5** has a good response to TNP. When adding 20μM TNP, the fluorescence intensity of **CS 5** solution has been quenched by 70%, which also shows that **CS 5** is very sensitive to TNP. The UV-Vis spectra also prove this. UV-Vis spectra of the probe solution added with TNP red-shifted from 372nm to 378nm, and the absorbance increased greatly. Although the spectra of the probe solution with 4-NP blue shifted from 372nm to 316nm, and the absorbance also changed slightly, the fluorescence spectra of the solution didn't change much, so **CS 5** can still be used as a fluorescent probe for detecting TNP.

The fluorescence response of probe **CS 5** upon adding TNP was discussed by titration spectra analysis. As illustrated in Fig. 6, as the concentration of TNP increases, the fluorescence intensity of the solution decreases. This can also be proved by photographs under the illumination of the ultraviolet lamp observed by the naked eye (Fig. S11). As expected, there is a good linear relationship between fluorescence intensity and TNP concentration in the range of 0 ~ 18μM. Subsequently, according to the formula, the LOD of TNP was calculated to be 0.81μM. Therefore, **CS 5** can also be used as a macromolecular sensor to detect the presence of TNP.

3.4. Detection mechanism

Due to the poor solubility of cellulose derivatives, as a reference molecule, small fluorescent probe molecules (**AC 2**, **AC 3**, **AC 4** and **AC 5**) were synthesized using n-butylamine instead of compound **CS 1**. Small molecule reference probes **AC 3** and **AC 4** were used to study the selective detection mechanism of aromatic nitro compounds. As shown in Fig. 7, when different analytes were added, **AC 3** and **AC 4** only showed obvious quenching reaction to TNP. Although small molecule probes also have specific detection ability for TNP, the sensitivity of small molecule probes is not enough. When the TNP concentration is 7 times the equivalent of the sensor (7×10^{-5} mol/L), the obvious quenching effect appears. In addition, the fluorescence of the **AC 3** solution is very weak, and it is almost invisible under ultraviolet light (Fig. S11). Therefore, grafting fluorescent probes onto the cellulose molecular chain increases fluorescence by aggregate induced emission (AIE) (Zhang et al. 2013). The more fluorescent units introduced to cellulose, the greater the sensitivity of the probe. This also proves that the cellulose fluorescent derivative does have the function of selectively identifying TNP, and further improves the sensitivity, which is conducive to the application and development of the detection of nitro-aromatic compounds.

In order to further reveal the process of TNP binding to the macromolecular sensors, we refer to the binding process of TNP and the small molecule probe **AC 3**. As shown in Fig. 7, ^{1}H NMR spectra of probe **AC 3** were taken in DMSO-d_6 in the presence of TNP. It can be seen that the peak at 3.3 ppm moved to the low field and peak broadening occurs, which may be the reason for the interaction with water. According to the literature, the chemical shift of Hp on TNP is above 9 ppm (Zhang et al. 2013). Once the interaction

between TNP and the sensor occurred, the proton signal on the aromatic ring of TNP will shift to the upper field. In Fig. 7, the chemical signal of TNP is at 8.55ppm, so it can be proved that TNP does interact with the sensor. Secondly, slight upfield shifts were observed for the proton signals of the benzene ring. These results indicate that after adding TNP, the naphthalimide probe interacts with TNP to a certain extent, resulting in fluorescence quenching. A reasonable explanation may be the use of photo-induced electron transfer (PET) mechanism to interact electron-deficient TNP compounds with electron-rich naphthalimide small molecules to generate electron transfer, thereby causing field shift and fluorescence quenching (Cao et al. 2017; Kundu et al. 2019; Ma et al. 2016). Similarly, the same is true for other small molecule sensors. Therefore, when a large number of naphthalimide electron-donating groups are connected to the cellulose chain, the macromolecular sensor can effectively combine with the electron-deficient nitrophenol to achieve the purpose of detection.

4. Conclusion

In summary, using naphthalimide as the fluorophore, cellulose based fluorescent probes were prepared. The as-prepared cellulose sensors have highly selective and sensitive ability to TNP. The best detection limit of three cellulose-based probes reaches 0.52μM. The selective detection of TNP by fluorescent cellulose derivatives is mainly due to the mechanism of photoinduced electron transfer (PET) and resonance energy transfer. By introducing electron-rich moieties of 2-mercaptobenzothiazole, benzothiazole-2-ylamine, 2-mercaptobenzimidazole, the polymeric sensors combine the electron-poor TNP easily. The cellulose-based fluorescent sensors exhibit selective and sensitive ability to TNP accordingly. By this modification of cellulose, the application scope of cellulose was enlarged.

Declarations

This work is approved by the Ethics Committee of Wuhan Institute of Technology; there are not any animal test in this work. The authors declare no competing financial interest.

Acknowledgement

The authors would like to thank the financial support of National Natural Science Foundation of China (NSFC, No. 41573106).

References

Abe M, Sugimura K, Nishiyama Y, Nishio Y (2017) Rapid Benzylation of Cellulose in Tetra-n-butylphosphonium Hydroxide Aqueous Solution at Room Temperature. ACS Sustain Chem Eng 5:4505-4510. https://doi.org/10.1021/acssuschemeng.7b00492

Bahta M, Ahmed N (2019) A novel 1,8-naphthalimide as highly selective naked-eye and ratiometric fluorescent sensor for detection of Hg^{2+} ions. J Photochem Photobiol A-Chem 373:154-161.

Barazzouk S, Daneault C (2011) Spectroscopic characterization of oxidized nanocellulose grafted with fluorescent amino acids. Cellulose 18:643-653. https://doi.org/10.1007/s10570-011-9503-5

Bora A, Mohan K, Dolui SK (2019) Carbon Dots as Cosensitizers in Dye-Sensitized Solar Cells and Fluorescence Chemosensors for 2,4,6-Trinitrophenol Detection. Ind Eng Chem Res 58:22771-22778. https://doi.org/10.1021/acs.iecr.9b05056

Cao XH, Zhao N, Lv HT, Ding QQ, Gao AP, Jing QS, Yi T (2017) Strong Blue Emissive Supramolecular Self-Assembly System Based on Naphthalimide Derivatives and Its Ability of Detection and Removal of 2,4,6-Trinitrophenol. Langmuir 33:7788-7798. https://doi.org/10.1021/acs.langmuir.7b01927

Cheng S, Liu Y, Zhao Y, Zhao X, Wang YH (2019) Superfine CoNi alloy embedded in Al_2O_3 nanosheets for efficient tandem catalytic reduction of nitroaromatic compounds by ammonia borane. Dalton Transactions 48:17499-17506. https://doi.org/10.1039/C9DT03838H

Choi SA, Park CS, Kwon OS, Giong HK, Lee JS, Ha TH, Lee CS (2016) Structural effects of naphthalimide-based fluorescent sensor for hydrogen sulfide and imaging in live zebrafish. Sci Rep 6:10. https://doi.org/10.1038/srep26203

de Faria AF, de Moraes ACM, Andrade PF, da Silva DS, Goncalves MD, Alves OL (2017) Cellulose acetate membrane embedded with graphene oxide-silver nanocomposites and its ability to suppress microbial proliferation. Cellulose 24:781-796. https://doi.org/10.1007/s10570-016-1140-6

Dhiman S, Kumar G, Luxami V, Singh P, Kumar S (2020) Stilbazolium dye based chromogenic and Red-fluorescent probe for recognition of 2,4,6-trinitrophenol in water. New Journal of Chemistry 44:10870. https://doi.org/10.1039/D0NJ00489H

Fan J, Zhang SF, Li F, Shi JW (2020) Cellulose-based sensors for metal ions detection. Cellulose 27:5477-5507. https://doi.org/10.1007/s10570-020-03158-x

Fuchs P, Zhang K (2019) Efficient synthesis of organosoluble 6-azido-6-deoxy-2,3-O-trimethylsilyl cellulose for click reactions. Carbohydr Polym 206:174-178. https://doi.org/10.1016/j.carbpol.2018.11.003

Guo MX, Yang L, Jiang ZW, Peng ZW, Li YF (2017) Al-based metal-organic gels for selective fluorescence recognition of hydroxyl nitro aromatic compounds. Spectrochimica Acta Part a-Molecular and Biomolecular Spectroscopy 187:43-48. https://doi.org/10.1016/j.saa.2017.05.057

Guo R, Gao L, Liang J, Zhang Z, Zhang J, Niu X, Hu T (2020) Two tetranuclear Cd-based metal-organic frameworks for sensitive sensing of TNP/Fe^{3+} in aqueous media and gas adsorption. Crystengcomm 22:6927-6934. https://doi.org/10.1039/d0ce01193b

Gupta AK, Tomar K, Bharadwaj PK (2017) Structural diversity of Zn(II) based coordination polymers constructed from a flexible carboxylate linker and pyridyl co-linkers: fluorescence sensing of nitroaromatics. New Journal of Chemistry 41:14505-14515. https://doi.org/10.1039/c7nj02651j

Hu HZ, Wang FY, Yu LS, Sugimura K, Zhou JP, Nishio Y (2018) Synthesis of Novel Fluorescent Cellulose Derivatives and Their Applications in Detection of Nitroaromatic Compounds. ACS Sustain Chem Eng 6:1436-1445. https://doi.org/10.1021/acssuschemeng.7b03855

Huang ST, Liu XH, Chang CY, Wang YX (2020) Recent developments and prospective food-related applications of cellulose nanocrystals: a review. Cellulose 27:2991-3011. https://doi.org/10.1007/s10570-020-02984-3

Imamura AH, Segato TP, de Oliveira LJM, Hassan A, Crespilho FN, Carrilho E (2020) Monitoring cellulose oxidation for protein immobilization in paper-based low-cost biosensors. Microchim Acta 187:8. https://doi.org/10.1007/s00604-020-04250-6

Jasmani L, Eyley S, Schutz C, Van Gorp H, De Feyter S, Thielemans W (2016) One-pot functionalization of cellulose nanocrystals with various cationic groups. Cellulose 23:3569-3576. https://doi.org/10.1007/s10570-016-1052-5

Kundu BK, Pragti, Reena, Mobin SM, Mukhopadhyay S (2019) Mechanistic and thermodynamic aspects of a pyrene-based fluorescent probe to detect picric acid. New Journal of Chemistry 43:11483-11492. https://doi.org/10.1039/c9nj02342a

Kusuma SBW, Hirose D, Takahashi K (2019) Transesterification Reaction of Cellulose with Inactive Esters in Ionic Liquids Acting as Both Catalysts and Solvents. Chem Lett 48:1122-1125. https://doi.org/10.1246/cl.190392

Li SY, Long T, Wang Y, Yang XG (2020) Self-assembly, protonation-dependent morphology, and photophysical properties of perylene bisimide with tertiary amine groups. Dyes Pigment 173:9. https://doi.org/10.1016/j.dyepig.2019.107896

Luo QB, He ZL, Xu WB, Shen H, Liang D, Ren T (2019) The spontaneous combustion mechanism of sawdust from the aspect of biochemical components. Cellulose 26:9045-9055. https://doi.org/10.1007/s10570-019-02697-2

Ma HW, He CY, Li XL, Ablikim O, Zhang ST, Zhang M (2016) A fluorescent probe for TNP detection in aqueous solution based on joint properties of intramolecular charge transfer and aggregation-induced enhanced emission. Sens Actuator B-Chem 230:746-752. https://doi.org/10.1016/j.snb.2016.02.112

Miao CL (2019) Design and construction of a 2D Pb-II coordination polymer as a multi-response luminescent sensor for Fe^{3+}, $Cr_2O_7^{2-}$, and TNP. J Mol Struct 1193:286-293. https://doi.org/10.1016/j.molstruc.2019.05.021

Navarro JRG, Bergstrom L (2014) Labelling of N-hydroxysuccinimide-modified rhodamine B on cellulose nanofibrils by the amidation reaction. RSC Adv 4:60757-60761. https://doi.org/10.1039/c4ra06559j

Peretz R, Mamane H, Sterenzon E, Gerchman Y (2019) Rapid quantification of cellulose nanocrystals by Calcofluor White fluorescence staining. Cellulose 26:971-977. https://doi.org/10.1007/s10570-018-2162-z

Qiu F, Huang YH, Ge QM, Liu M, Cong H, Tao Z (2020) The high selective chemo-sensors for TNP based on the mono- and di-substituted multifarene 2,2 with different fluorescence quenching mechanism. Spectrochimica Acta Part a-Molecular and Biomolecular Spectroscopy 226:6. https://doi.org/10.1016/j.saa.2019.117583

Ruiz-Sanchez AJ, Collado D, Mayorga C, Torres MJ, Perez-Inestrosa E (2020) Naphthalimide Dyes with Orthogonal Functional Groups for "Click" Chemistry: Attachment to Solid Supports and Applications in Drug Allergy Diagnosis. ChemPlusChem 85:689-693. https://doi.org/10.1002/cplu.202000118

Saini V, Gupta A, Rangan K, Khungar B (2020) A selective turn-off fluorescence detection of nitroexplosive 2,4,6-trinitrophenol by pyridinium-based chemosensor in pure aqueous medium. Dyes Pigment 180:9. https://doi.org/10.1016/j.dyepig.2020.108447

Sharma P, Mehata MS (2020) Colloidal MoS_2 quantum dots based optical sensor for detection of 2,4,6-TNP explosive in an aqueous medium. Opt Mater 100:5. https://doi.org/10.1016/j.optmat.2019.109646

Song RY, Zhang Q, Chu YL, Zhang L, Dai HQ, Wu WB (2019) Fluorescent cellulose nanocrystals for the detection of lead ions in complete aqueous solution. Cellulose 26:9553-9565. https://doi.org/10.1007/s10570-019-02760-y

Tripathi N, Singh P, Kumar S (2017) Dynamic fluorescence quenching by 2,4,6-trinitrophenol in the voids of an aggregation induced emission based fluorescent probe. New Journal of Chemistry 41:8739-8747. https://doi.org/10.1039/c7nj01277b

Wang J, Liu ZT, Shao XY, Hu N, Liu M, Xu YW (2020a) A novel preparation method and characterization of fluorescent cellulose fibers. Cellulose 27:3651-3659. https://doi.org/10.1007/s10570-020-03062-4

Wang J, Zhong Y, Bai C, Guan Y, Hu HM (2020b) Series of coordination polymers with multifunctional properties for nitroaromatic compounds and Cu II sensing. Journal of Solid State Chemistry 288:121381. https://doi.org/10.1016/j.jssc.2020.121381

Xiao YJ, Yang XQ, Cheng XJ, Xiong SY, Chen R (2020) Fluorescent macromolecular chemosensors for highly and selectively detecting of 2, 4, 6-trinitrophenol. Mater Res Express 7:14. https://doi.org/10.1088/2053-1591/abbbab

Xiong FQ, Han YM, Li GY, Qin TF, Wang SQ, Chu FX (2016) Synthesis and characterization of renewable woody nanoparticles fluorescently labeled by pyrene. Ind Crop Prod 83:663-669. https://doi.org/10.1016/j.indcrop.2015.12.055

Xiong SY, Marin L, Duan L, Cheng XJ (2019) Fluorescent chitosan hydrogel for highly and selectively sensing of p-nitrophenol and 2, 4, 6-trinitrophenol. Carbohydr Polym 225:10. https://doi.org/10.1016/j.carbpol.2019.115253

Xu Y, Guo Y, Zhang J (2020) A fluorescent coordination polymer for TNP detection and protection effect on cough after infection by up-regulates the activity of neuroendopeptide enzyme in respiratory tract mucosa. Journal of Polymer Research 27. https://doi.org/10.1007/s10965-020-02299-8

Yang Y et al. (2019) Rhodamine B assisted graphene quantum dots flourescent sensor system for sensitive recognition of mercury ions. J Lumines 207:273-281. https://doi.org/10.1016/j.jlumin.2018.11.033

You J, Hu H, Zhou J (2013) Synthesis, structure and solution properties of the novel polyampholytes based on cellulose. Cellulose 20:1175-1185. https://doi.org/10.1007/s10570-013-9891-9

Zhang F et al. (2013) Synthesis of a novel fluorescent anthryl calix 4 arene as picric acid sensor. Tetrahedron 69:9886-9889. https://doi.org/10.1016/j.tet.2013.08.083

Figures

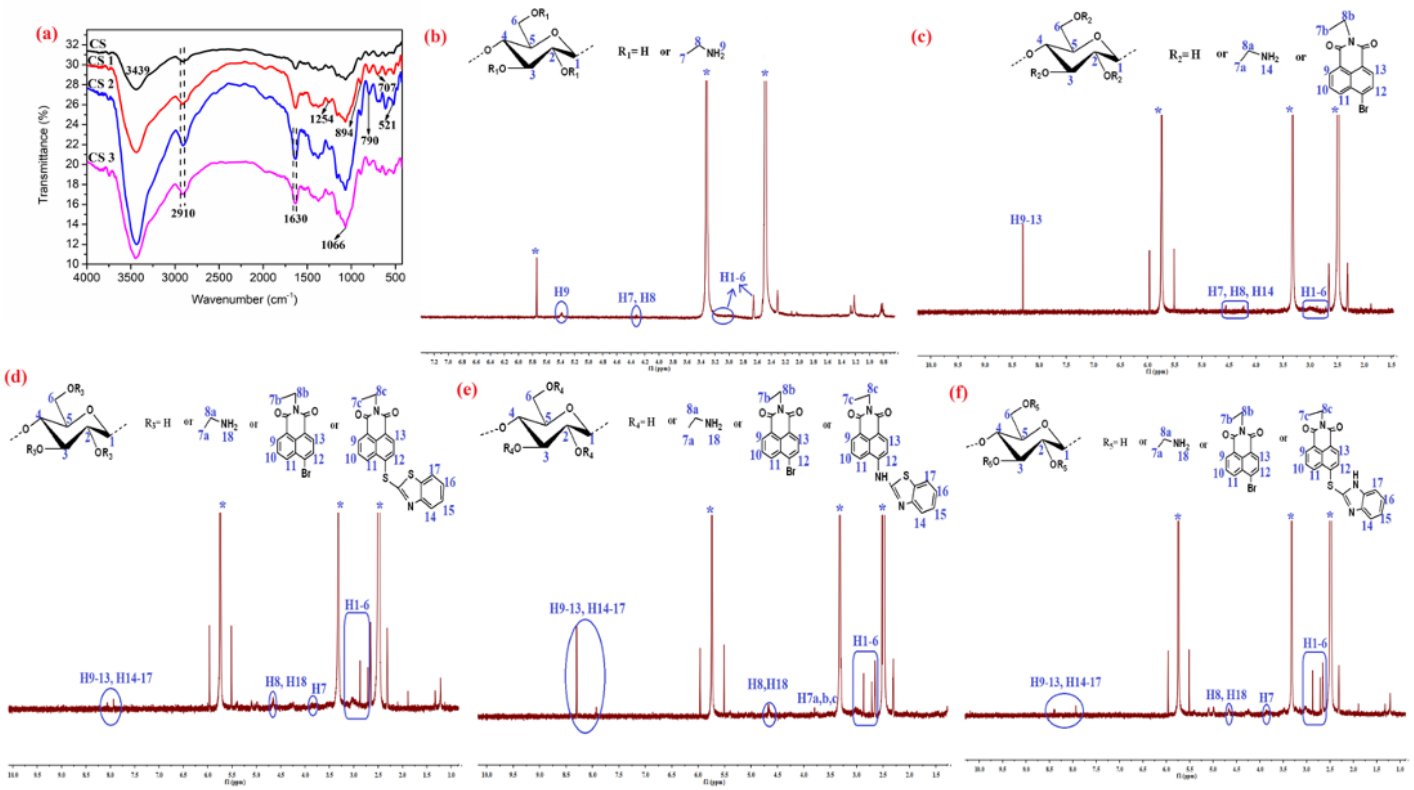

Figure 1

FT-IR spectra of (a) CS, CS 1, CS 2 and CS 3, 1H NMR spectra of (b) CS 1, (c) CS 2, (d) CS 3, (e) CS 4 and (f) CS 5

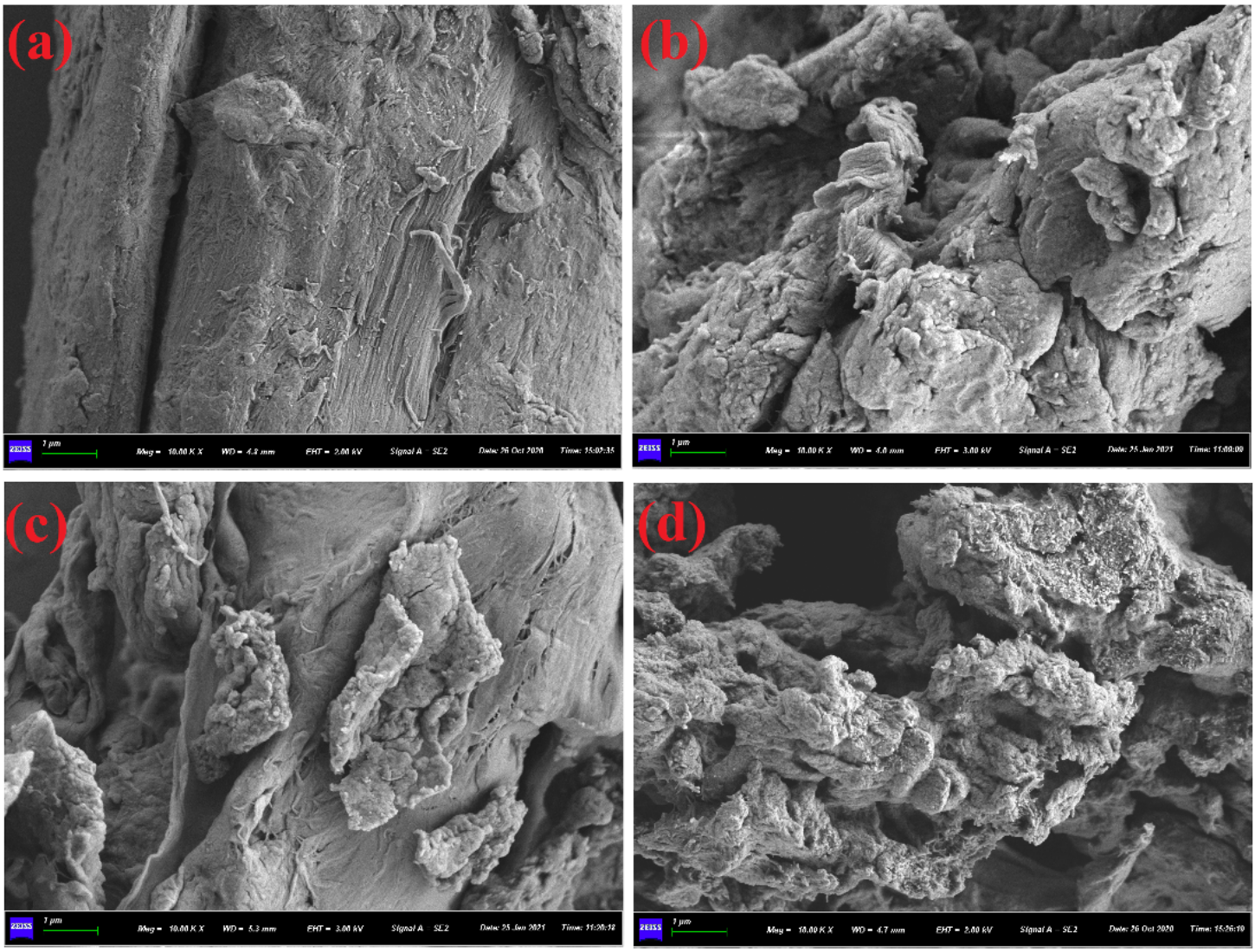

Figure 2

SEM micrograph of celluloses (a) and modified cellulose derivatives (b) CS 1, (c) CS 2, (d) CS 3, The scale bars for samples are 1 µm

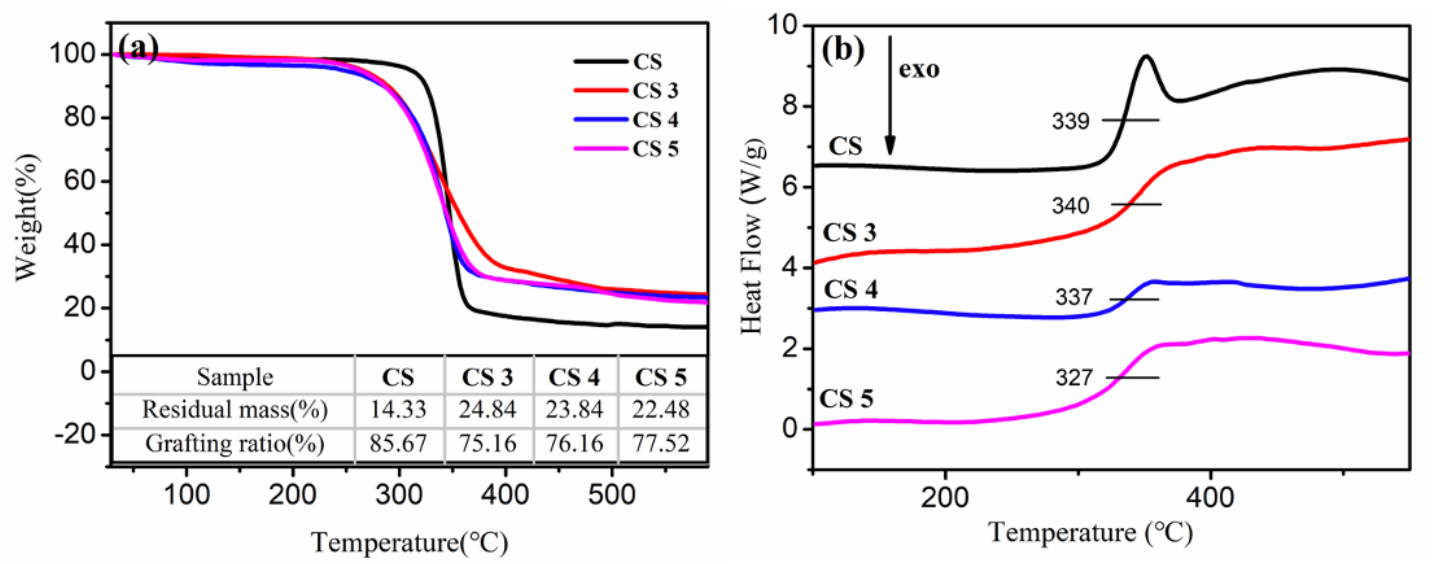

Figure 3

(a) TGA and (b) DSC of cellulose (CS) and its derivatives CS 3, CS 4 and CS 5. Inset of (a) is residual mass and grafting ratio of CS, CS 3, CS 4 and CS 5

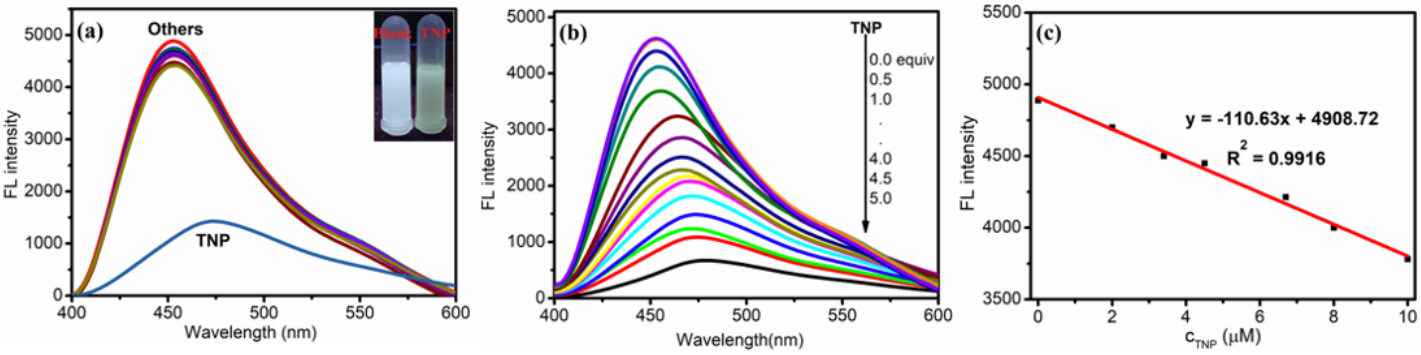

Figure 4

(a) Fluorescence spectra (λex=365 nm) of CS 3 (2mg/3mL) in the presence of 2 equivalent of nitro compounds (50μM) in DMSO. Insert: photograph of blank sample with TNP under fluorescence. (b) Fluorescence intensity changes of sensors with different equivalent of TNP (from 0 to 5 equivalent), when λex= 365 nm. (c) Standard curve for fluorescence titration of sensor with TNP.

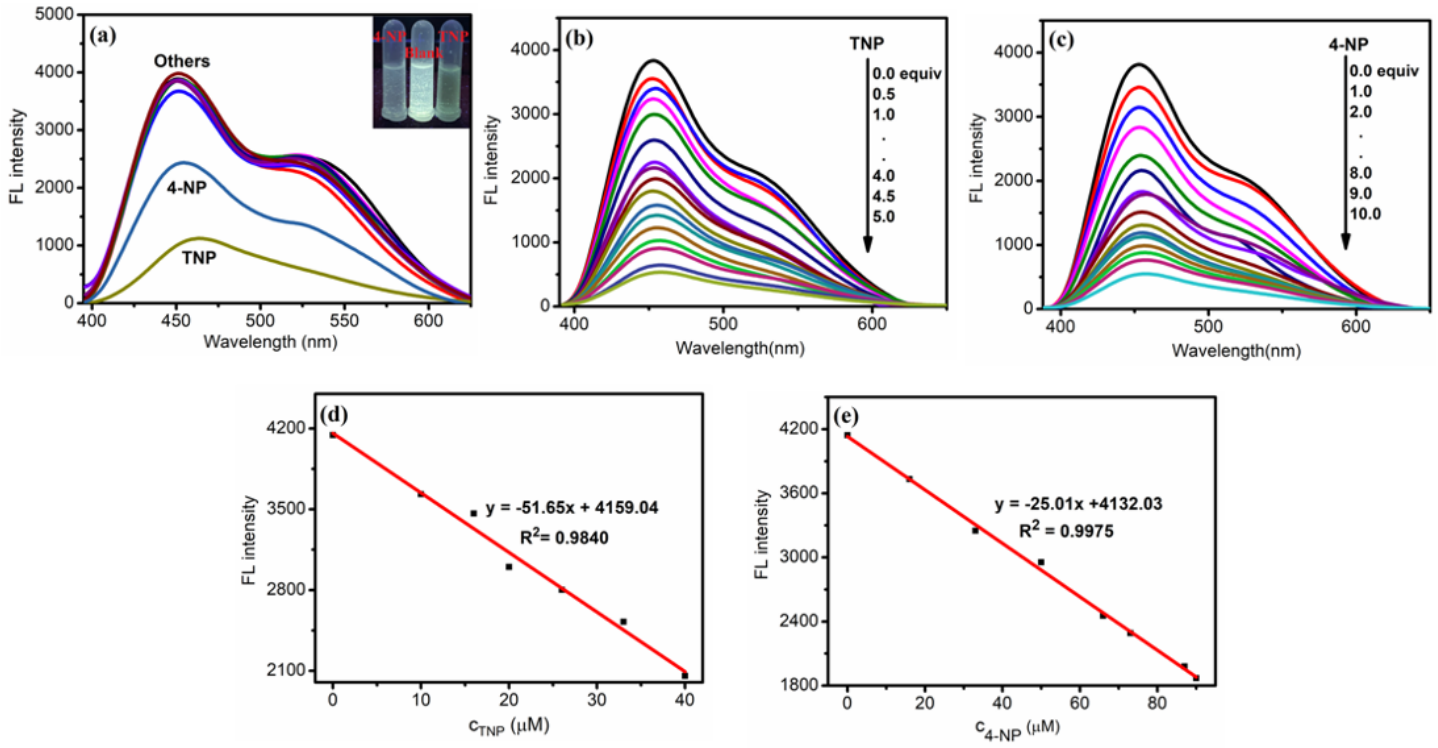

Figure 5

(a) Fluorescence spectra (λex=365 nm) of CS 4 (2mg/3mL) in the presence of 2 equivalent of nitro compounds in mixed solvent (glycerol: ethanol=3: 4). Insert: photograph of 4-NP and TNP with blank sample under fluorescence. Fluorescence intensity changes of sensors with different equivalent of (b) TNP (from 0 to 5 equivalent) and (c) 4-NP (from 0 to 10 equivalent), when λex= 365 nm. Standard curve for fluorescence titration of sensor with (d) TNP and (e) 4-NP

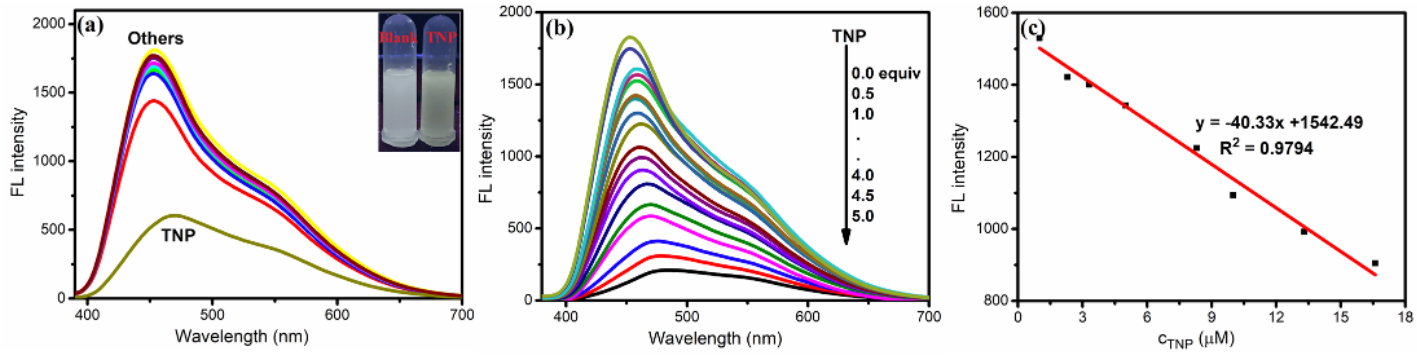

Figure 6

(a) Fluorescence spectra (λex=365 nm) of CS 5 (2mg/3mL) in the presence of 2 equivalent of nitro compounds in DMSO. Insert: photograph of TNP with blank sample under fluorescence. (b) Fluorescence

intensity changes of sensors with different equivalent of TNP (from 0 to 5 equivalent), when λex= 365 nm. (c) Standard curve for fluorescence titration of sensor with TNP.

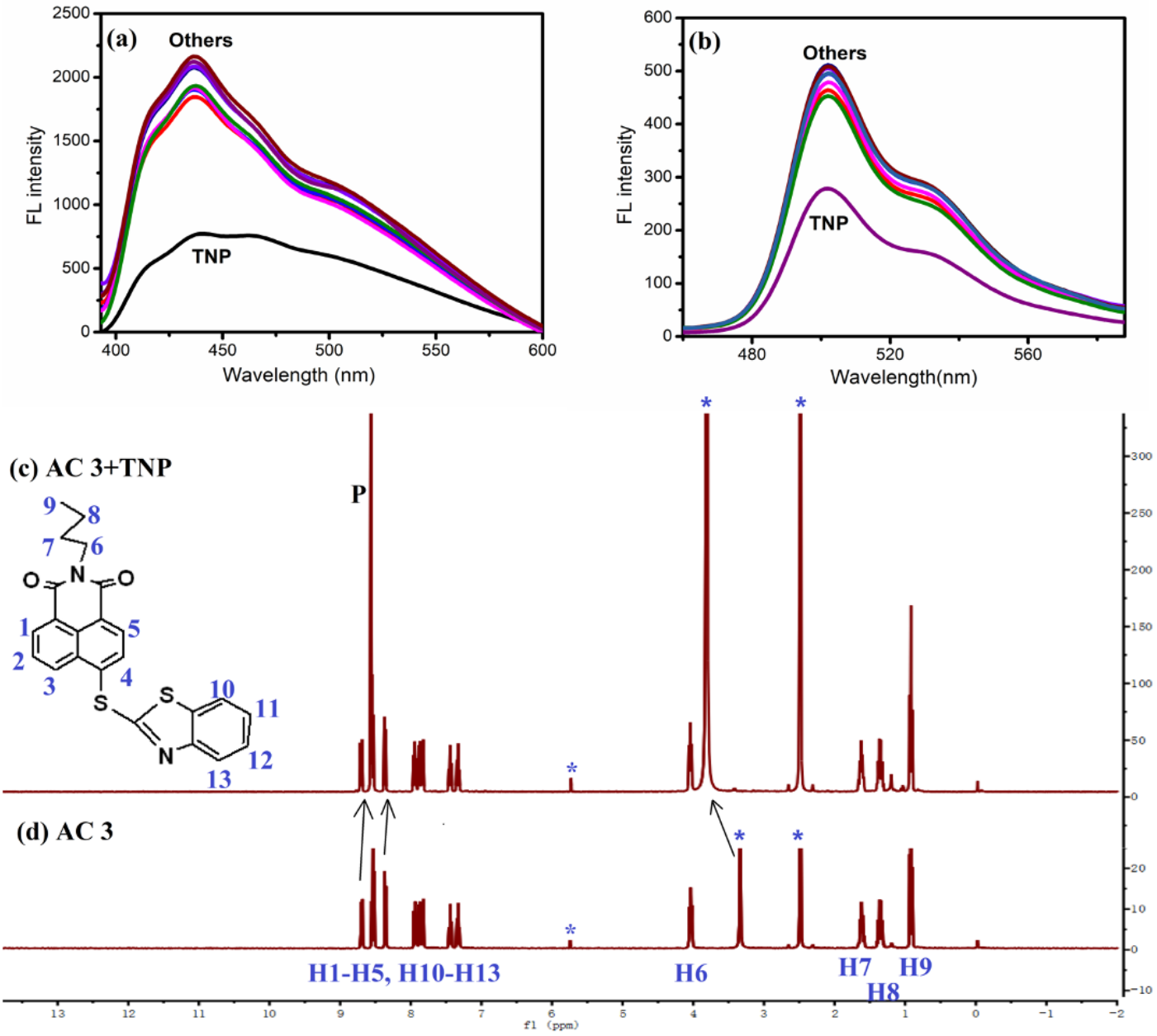

Figure 7

Fluorescence intensity change of (a) AC 3, (b) AC 4 (10-5 mol/L) in CH3CN after addition of nitro compounds (7×10-5 mol/L). when λex = 365 nm. Insert: photograph of blank sample with TNP under fluorescence. 1H NMR spectra of AC 3 (c) with and (d) without TNP in DMSO-d6

Supplementary Files

This is a list of supplementary files associated with this preprint. Click to download.

- GraphicalAbstract.png
- Scheme1.png
- Scheme2.png
- SupportingMaterials.docx